JAAS

Measurements of mass-dependent Te isotopic variation by hydride generation MC-ICP-MS

Journal:	*Journal of Analytical Atomic Spectrometry*
Manuscript ID	JA-ART-07-2019-000244.R2
Article Type:	Paper
Date Submitted by the Author:	23-Nov-2019
Complete List of Authors:	Wasserman, Naomi; University of Illinois at Urbana-Champaign, Geology Johnson, Thomas; University of Illinois at Urbana-Champaign, Geology

N.L Wasserman
4042 Natural History Building
1301 W. Green St.
Urbana, IL 61801
Email: nwasser2@illinois.edu

Measurements of mass-dependent Te isotopic variation by hydride generation MC-ICP-MS

N.L. Wasserman and T.M. Johnson

Department of Geology, University of Illinois at Urbana-Champaign
Natural History Building
1301 W. Green St.
Urbana, IL 61801

Measurements of mass-dependent Te isotopic variation by hydride generation MC-ICP-MS

Naomi L. Wasserman and Thomas M. Johnson

Abstract

Tellurium (Te) stable isotope measurements have the potential to serve as tracers of Te mobility and redox conditions in modern and ancient environments. Here, we present a method to measure Te isotope ratios by MC-ICP-MS utilizing a hydride generation system to efficiently deliver Te to the plasma, in combination with a ^{120}Te-^{124}Te double spike. This approach allows for precise $\delta^{130}Te/^{126}Te$ (2σ: 0.09‰) measurements while using less than 8.75 ng of natural Te. Although hydride generation methods usually produce higher sensitivity than more conventional methods, for Te, the sensitivity is similar, on our instrument, to that achieved using a desolvating nebulizer. Nonetheless, hydride generation has an advantageous ability to exclude interfering elements such as Ba and allow analysis of samples without chemical separation of Te in some cases. We also demonstrate successfully a modified ion exchange procedure to separate various matrix components and isobaric interferences from Te in natural sediments. Analyses of multiple digestions of USGS standard reference materials, mine tailings, ancient sediments, and soils utilizing this approach show the largest spread in terrestrial Te isotopic composition to date ($\delta^{130}Te/^{126}Te$ ~1.21‰) and a lack of detectable mass-independent fractionation.

1.1 Introduction

Tellurium (Te) is an economically valuable metalloid often incorporated into photovoltaic cell technology and nanotechnology.[1] Estimates show that demand for Te may increase as much as 100-fold by 2030, and this may lead to increasing instances of mining-related contamination as observed around Cu smelters (Canada) and a nickel refinery (UK).[2,3] Exposure to high concentrations of Te can result in liver and kidney necrosis and collapse of the respiratory and circulatory systems.[4, 5] Tellurium is currently extracted primarily as a byproduct of copper solvent extraction-electrolytic refining.[1] This method will most likely be phased out due to more efficient solvent extraction methods for copper refining that do not involve Te separation.[3] Accordingly, both exploration for Te ores and increased occurrence of industrial Te contamination may occur, and there is a greater need to examine low-temperature abiotic and microbial processes that control Te enrichment in ores, and Te transport in contaminated water.

While Te has a low crustal abundance (~1-3 ng g^{-1})[6], certain geochemical processes can concentrate Te. A compilation of soil and sediment samples indicates that Te concentrations range from less than 5 to 100 ng g^{-1} and past studies have see enrichments up to 50,000 times in ferromanganese crusts.[7,8] Similar to other group 16 elements, selenium and sulfur, Te is found in four nominal oxidation states (-2, 0, +4, +6). Tellurium can be mobile in the +4 and +6 states as a soluble oxyanion, whereas in the reduced states it tends to have low solubility, forming solid tellurides or elemental Te nanorods.[3] In oxic marine surface waters, Te(IV) and Te(VI) exist as oxyanions in roughly equal proportions.[9] Both the irregularly-coordinated tellurite (TeO_3^{2-}) and octahedrally-coordinated tellurate (TeO_4^{2-}) species are scavenged by Fe- and Mn-oxy(hydrox)ides, although tellurite adsorbs more strongly.[10] Unlike Se, Te is not a micronutrient. Several studies, though, have observed microbial dissimilatory reduction of Te(IV) and Te(VI) to Te(0) nanorods or methylated tellurides.[11, 12]

Because a variety of abiotic and microbially-mediated redox processes influence Te mobility, there is increasing interest to develop the element as an indicator of paleoredox conditions. Decades of studies have utilized various isotopic and chemical proxies to provide constraints on the relative oxidizing power of the atmospheric and oceanic systems. Geochemical redox proxies indicate that, from the Great Oxygenation Event (~2.4 Ga) until

the next major oxygenation event at 0.8 Ga, atmospheric oxygen remained low, while certain portions of the ocean (shallow oases and deep marine environments) may have been partially oxygenated.[13-15] Such decoupling highlights the need for the development of additional geochemical tools, like Te isotopes, to trace distinct redox conditions of marine and terrestrial environments.

With eight stable isotopes, Te stable isotope measurements may be useful as tracers of redox processes that affect Te mobility. Similar to the Se, Cr, and U isotope systems, Te mass-dependent isotopic fractionation may occur during reduction or oxidation by abiotic or biological reactants.[16-18] Theoretical calculations by Smithers and Krause[19] estimated a 6‰ difference between $^{130}Te/^{125}Te$ of TeO_4^{2-} and H_2Te at isotopic equilibrium.[19] Baesman et al.[11] observed a kinetic Te isotopic fractionation factor of $\varepsilon \sim -2.0$ to -5.0‰ in laboratory reduction of TeO_4^{2-} and TeO_3^{2-} by sulfite, cysteine, and two bacterial cultures amended with acetate.[11] The fractionation factor, ε, is equivalent to 1000‰ x (α-1), where α equals the ratio of the $^{130}Te/^{125}Te$ of the instantaneous product relative to the reactant. Recent surveys of Te ores (range of ~2‰) and ordinary chondrites (range of ~6.3‰) and sediments (range of ~0.85‰) also show significant isotopic fractionation.[20-22] However, attempts to examine isotopic variation in soil samples (typically <20 ng mL^{-1}) have been limited by the inability of analytical techniques to measure the very small masses found in many materials.

Here, we present a method for Te stable isotope measurements that allows for small masses of natural Te (<8.75 ng) without a need for a Ba correction, using a hydride generation sample introduction system in combination with a ^{120}Te-^{124}Te double spike. We also present an ion exchange purification technique modified from previous studies to achieve high recovery while separating Te from typical sample matrix components (e.g., Fe) and isobaric interferences (e.g., Sn).[23,24] With this method, the Te isotope approach can be more broadly applied to improve understanding of modern contaminated systems, paleoredox states of ancient earth systems, igneous systems, and modern critical zone processes.

2. Experimental

2.1 Reagents

Acids for digestion and chemical separation of samples were prepared from American Chemical Society (ACS)-Certified HCl (Macron Fine Chemicals), ACS-Certified HNO_3

(Fisher Chemical), and HF (99.99% purity, Alfa Aesar). Additional distillation was not required as the acid blanks contained less than 0.1 ng mL^{-1} Te. The oxidizing solution for Te was prepared with potassium persulfate (Certified ACS, Fisher) powder. A Millipore Milli-Q Integral water purification system (Merck Millipore, USA) provided ultrapure water (18.2 MΩ) with which all reagent solutions were made. $NaBH_4$ (>98%, Acros Organics) and NaOH (Certified ACS, Fisher) powdered reagents were utilized to prepare the reductant solution used for hydride generation.

2.2 Samples and standards

Three Te standards, National Institute of Standards and Technology (NIST) SRM 3156 Te concentration standard (Lot no. 140830), Alfa Aesar Na_2TeO_3 powder reagent (99.5% metals basis, lot no. M27C052), and Alfa Aesar $H_2TeO_4 \bullet 2H_2O$ powder reagent (99% metals basis, lot no. Y05A029), were used to evaluate long-term precision. Single batches of these stock solutions of these reagents were used as in-house standards to assess precision. All solutions were prepared by dissolving the powder in 1 M HCl. A Te standard solution in 5% HNO_3 (Spex CertiPrep) was used as a concentration standard for measurements by single collector inductively coupled plasma-mass spectrometry (ICP-MS) (Thermo Scientific, iCAP Q).

Seven United States Geological Survey geochemical reference materials were digested and measured. Three of these standards, Nod-P-1, SGR-1 and MAG-1 have been measured previously.[20, 21] Briefly, Nod-P-1 is a diagenetic manganese nodule from the Pacific Ocean, SGR-1 is a shale powder from the Green River Formation, and MAG-1 is a marine mud from the Wilkinson Basin, Gulf of Maine.[25,26] The USGS standard SCO-1, an Upper Cretaceous silty marine shale, has no published Te isotope values.[26] One USGS soil sample, C-320293, is a topsoil taken from shrubland in the Humboldt-Toiyabe Forest in Nevada, USA.[27]

Several mine tailings were collected from millsites from across the western United States with all coordinates recorded using NAD83 spheroid and WGS84 datum. The Delamar mining district (Lincoln County, NV; coordinates: 37.45892, -114.77739) was mined for gold from 1892 through 1909 leaving at least 408,000 metric tons of mine tailings at the site.[28] Sample "Delamar big tailings surface" (0-2 cm) was collected from the site, "big

tailings pile". This site was characterized by smaller particle sizes, higher extent of oxidation, and higher concentrations of potentially toxic elements.[29] The Ute Ulay mill (Hinsdale County, CO; coordinates: 38.0192289, -107.3768862) intermittently processed lead and zinc ore since 1874. More recently, tailings from the Golden Wonder, a nearby gold telluride deposit, have been deposited at the site since the 1990's.[30] Samples, "Ute Ulay surface" (0-2 cm) and "Ute Ulay deep" (83-90 cm), were collected from a fresh tailings pit there. Sample "Vulcan precipitate" is a precipitate found in weathered mine tailings, dominantly copiapite ($Fe^{2+}Fe^{3+}_4(SO_4)_6(OH)_2 \bullet 20H_2O$), collected from the soil surface under the historic Vulcan mill structure (Gunnison County, CO; coordinates: 38.3447176, -107.0062077). Sample "Masonic surface" (0-2 cm) was collected from the streambed just downstream of the historic Masonic Mill (Mono County, CA; coordinates 38.3673, -119.12059).

Two ancient sediments were also digested. The first sample "CLRD-3.0" is from the 2.45 Ga Cooper Lake paleosol (Ontario, Canada). The paleosol, made up of dominantly quartz and clay minerals with lesser amounts of pyrite, is developed on the Algomon granite at the base of the Huronian Supergroup[31]. It is interpreted to have formed under anoxic atmospheric conditions[32]. The second sample (CLG-1) originates from the 1.650 Ga Mesoproterozoic Chuanlinggou Formation (Northern China).[33] It is composed of primarily oolitic iron deposits, which were deposited in a ferruginous and mildly oxic water column[34].

2.3 Digestion and purification

For samples with lower concentrations of Te (CLRD-3.0 and CLG-1) up to 0.4 g of sample was digested, while 0.02 g of "Masonic Surface", "Vulcan Yellow Precipitate", and "Delamar big tailings surface" samples was used. For all other samples approximately 0.2 g was used for digestion. Depending on the mass required, samples were digested in 4 or 8 mL reverse aqua regia (1:3 HCl: HNO_3 ratio) on a hot plate at 110°C for 24 hours. This digestion procedure was sufficient to release Te associated with non-silicate phases (e.g clays, sulfides, Fe-oxyhydroxides), which are present in all of the samples. For silicate-rich matrices reverse aqua regia has been adequate to release 85% to 100% of the Te present due to its association with sulfide and oxide phases[35]. Therefore, the small contribution of silicate phases in our samples should not influence our recovery. Residual solids were separated from the

supernatant, which was evaporated to dryness at 90°C. Unlike Se, where >80% of Se can be volatilized during evaporation in HCl matrices, little volatilization of Te occurs in HCl or HNO_3 at this temperature.[36] Small losses of Te by volatilization and possible isotopic fractionation are corrected by the Te double spike addition prior to digestion. Subsequently, the samples were brought up in 4 mL 6 M HCl and heated on the hot plate at 110°C for 2 hours to ensure all Te was converted to Te(IV). The ^{120}Te-^{124}Te double spike (+4 valence; see section 2.4) was added to the samples before digestion.

All chemical purification was performed in laminar flow HEPA-filtered clean hoods contained in a Class 10,000 Clean Lab (University of Illinois at Urbana-Champaign). The mass of Te loaded on the column ranged from 8 to 300 ng Te. For samples requiring more than 0.5 g of digested material (<15 ng Te), parallel column separations can be utilized with the expectation of a higher blank contribution. Separation from the majority of the interfering elements (Fe, matrix) was achieved using AG1-X8 anion exchange resin columns (3 mL bed volume; 100-200 mesh, BioRad Laboratories) following a modified procedure from Fehr et al.[37] and Wang and Becker[23]. Briefly, resin was conditioned in a Poly-Prep 10 mL column (BioRad Laboratories) with 8 mL 6 M HCl after which the sample was loaded, with Te retained. The column was rinsed with 6 mL of 6 M HCl to elute Se and other matrix elements (Co^{2+}, Ni^{2+}, Cu^{2+}, and Pb^{2+}) followed by 5 M HF, which removed most of the Fe, a suppressant of H_2Te formation during hydride generation.[38] Subsequently, 4 mL 9 M HCl was added to further elute matrix elements. To remove residual Fe, 5 mL of 2 M HCl was added before eluting Te(IV) with 8 mL of 1 M HNO_3.

Samples were evaporated to dryness at 90°C and further digested with five drops of concentrated HNO_3 followed by five drops of concentrated HCl. Once dried down, the residue was dissolved in 0.1 M HCl containing freshly made 0.02 M $K_2S_2O_8$. Samples were heated on a hot plate at 110°C for 90 minutes, converting all Te(IV) to Te(VI). After oxidation, samples were further purified with a 1 mL cation exchange column (AG50W-X8, 200-400 mesh, BioRad Laboratories) to remove Sn and Fe in a 10 mL Poly-Prep column (BioRad Laboratories). The columns were conditioned with 0.1 M HCl, after which, the sample was loaded followed by 5 mL of 0.1 M HCl. The eluent was immediately collected,

as H_2TeO_4 is a neutrally charged species and does not adsorb to the resin. Residual Fe(III) was retained on the column along with most of Sn(IV) at dilute HCl concentrations.[37] Once dried down, samples were again digested with 2 drops of concentrated HNO_3 followed by concentrated HCl.

In some cases, to further remove Sn from samples, samples were acidified to 0.4 M HCl and passed through a BioRad column following a modified procedure from Wang et al.[39]. A 1 mL AG1-X8 (100-200 mesh) resin bed was conditioned with 10 mL 0.4 M HCl. Once the sample was loaded, as Te(VI), the elutant was collected immediately along with the next 5 mL of 0.4 M HCl. The sample was then dried down, dissolved in 2 mL 5 M HCl and heated at 110°C for at least 2 hours to fully reduce Te(VI) to Te(IV).

2.4 Double spike

A ^{120}Te-^{124}Te double spike (2% HNO_3) was used to correct for instrumental mass bias and any isotopic fractionation that might occur during sample preparation. Double spike addition is a well-established method to precisely correct for instrumental mass bias.[40-42] ^{120}Te and ^{124}Te were chosen as the spike isotopes based on the minimization of error.[43] The isotopic composition of the double spike was determined by hydride generation measurements, corrected for mass bias determined from NIST SRM 3156 measurements before and after the double spike. The double spike composition was corrected for Sn and Xe interferences. Memory of the natural Te standard was removed completely before double spike measurement. The Te spikes were of high purity, containing 98.8% ^{120}Te and 93.0% ^{124}Te. The spikes were mixed to create solution with 54.40% ^{120}Te and 43.60% ^{124}Te (on a molar basis), which is close to the optimal ratio determined using the methods of Rudge et al.[36] (57% and 43%) using ^{126}Te and ^{130}Te as the inversion isotopes. The concentration of the double spike solution was calibrated based on measurements of a spiked Te concentration standard (Spex CertiPrep).

2.5 Mass spectrometry

All measurements were made on a Nu Plasma HR MC ICP-MS (Nu Instruments, UK) in low-resolution mode, with Te introduced to the plasma via a custom –built hydride generation system. The system generates $H_2Te_{(g)}$ by reacting Te(IV) in 4 M HCl (1.0 mL

min^{-1}) with an inline solution of 0.2 wt. % $NaBH_4$ and 0.2 wt. % NaOH (0.5 mL min^{-1}). A frit-based gas-liquid separator with an Ar flow of about 0.03 L min^{-1} stripped the H_2Te from the liquid, which was then passed through a 0.2 μm polytetrafluoroethylene (PTFE) filter to remove aerosols, and merged into Ar carrier gas (1.4 L min^{-1}). This allows for an efficient transfer of the gaseous H_2Te into the mass spectrometer. Importantly, only elements that can form gaseous hydrides and other volatile species can be transferred into the mass spectrometer through this method, excluding many potential isobaric interferences such as Ba, and molecular interferences from Mo, Nb, Zr, Cd, Pd, and Sr.

Several analyses were made using a desolvating nebulizer (CETAC, Aridus II DSN) to assess the advantages and disadvantages associated with each technique. A nebulizer Ar gas flow 1.0 L min^{-1} and sweep gas flow of 9.63 L min^{-1} allowed for a 0.07 mL min^{-1} sample uptake rate using a PFA MicroFlow nebulizer (Elemental Scientific).

The measurement routine used Faraday collectors on the Nu Plasma as shown in Table 1. Collectors were connected to amplifiers with standard 10^{11} Ω resistors on all collectors except the one in the H5 position (^{130}Te) which has been fitted with a 10^{10} Ω resistor. This facilitates high-precision ^{238}U/^{235}U measurements by allowing measurement at high ^{238}U intensities (up to 10^{-9} A). Unfortunately, reverting to the 10^{11} Ω resistor was not feasible during the course of this study and this resulted in greater baseline noise in the ^{130}Te measurement (see discussion). The measurement routine was set up such that ^{124}Te is in the Axial position (Table 1). In L4, ^{118}Sn, a common impurity in samples and the $NaBH_4$ reagent, is monitored to enable corrections for Sn interferences on ^{120}Te and ^{124}Te. SnH^+ sourced from the $NaBH_4$ was subtracted by on-peak zeroes, while that from the samples was such that ^{120}Sn/^{120}Te <0.02. In addition, ^{132}Xe was measured on collector H6 to enable correction for small Xe interferences on ^{130}Te, ^{128}Te, ^{126}Te and ^{124}Te. Baseline analysis of mass 120 without hydride generation revealed a ^{40}Ar^{40}Ar^{40}Ar interference of 2-3 mV, which was corrected for by on-peak zeroes. While we found no evidence for a significant SbH^+ interference on mass 124, mass 123 (^{123}Sb and ^{123}Te) was monitored. A TeH^+ correction removed hydride interferences on ^{125}Te and ^{126}Te. After each measurement, ^{124}Te^{1}H$^+$ or ^{125}Te^{1}H$^+$ was subtracted based on the intensity of ^{124}Te and ^{125}Te and a constant TeH^+/Te. At the beginning of each session, overspiked and underspiked samples were measured to validate and/or adjust the TeH^+/Te used for the correction. ^{125}Te is particularly sensitive to the TeH^+ interference, as the

contribution of $^{124}TeH^+$ derived from the relatively high-intensity spike isotope, ^{124}Te, strongly impacts the somewhat rare ^{125}Te isotope. Given the average TeH^+/Te of 0.0001, $^{123}TeH^+$ interference on ^{124}Te was not corrected for, as $^{123}TeH^+$ at normal intensities and spike to sample ratios would be less than 0.002‰ of the intensity of the ^{124}Te signal. ^{130}Ba and ^{132}Ba, while of low abundance, can be significant interferences on ^{130}Te and ^{132}Xe as observed by Fehr et al.[20] and Fukami et al.[21]. Similar to Brennecka et al.[38], we did not observe significant ^{137}Ba above baseline values during hydride generation for samples containing up to 1V on ^{137}Ba while using the DSN. Ba does not readily form hydrides in the conditions utilized and was not corrected for in our sample routine.

Interferences were partially corrected by subtraction after on-peak baseline and background measurements of a blank 4 M HCl solution with an integration time of 100 sec, immediately prior to peak centering on ^{128}Te and sample measurement. Residual Xe and Sn were further subtracted by measuring ^{132}Xe and ^{118}Sn during each integration of sample measurement and calculating the interferences using assumed natural isotopic compositions and the mass bias determined from the double spike. This was done in an iterative way as part of the double spike data reduction, so the interferences were accounted for in the mass bias determinations and vice-versa. Samples were measured over 5 blocks of 10 measurements, each integrated over 3 seconds. A total of 3.5 minutes of sample consumption time was required, followed by 6.6 minutes rinse time before the next analysis.

In order to compare our results to previous studies, we normalized our samples to NIST SRM 3156. While previous studies have reported the isotope ratio $^{130}Te/^{125}Te$, we report the ratio $^{130}Te/^{126}Te$ due to its lesser uncertainty: ^{126}Te is 2.7 times more abundant than ^{125}Te and the smaller measurement uncertainty using ^{126}Te more than compensated for the lower sensitivity of the $^{130}Te/^{126}Te$ ratio (4 D mass difference) to a given fractionation relative to the $^{130}Te/^{125}Te$ ratio (5 D mass difference). An analysis of counting statistics-related noise and baseline noise[20, 21, 38] revealed that $^{130}Te/^{125}Te$ should have an uncertainty 1.6x larger than $^{130}Te/^{126}Te$ at normal intensity. We observed that on average the uncertainty of $\delta^{130}Te/^{125}Te$ was 1.5 times that of $\delta^{130}Te/^{126}Te$ over 4 analytical sessions. In addition to $\delta^{130}Te/^{126}Te$, $\delta^{128}Te/^{126}Te$ and $\delta^{125}Te/^{126}Te$ were also determined independently to monitor for certain analytical problems such as uncorrected Xe, Sn, and hydride ($^{124}TeH^+$ and $^{125}TeH^+$) interferences. Over an analytical session, rejection of an analysis due to large

uncorrected Xe, Sn, or hydride residuals was uncommon once samples were effectively separated from Sn (see Section 3.5).

Standards and samples were spiked based on the optimal molar proportion of spike to sample ~0.98 as discussed in Section 3.3. All standards, once spiked, were heated in 5 M HCl at 100°C for 2 hours to reduce Te(VI) to Te(IV). High-precision measurements typically required a natural Te concentration of 2.5 ng mL^{-1}. All bracketing standards were diluted such that ^{130}Te measured to ~1.5V, while all samples were diluted such that ^{130}Te was 1.2 – 2 V. Given the 3.5 minutes required for measurement, one sample measurement typically consumed 8.75 ng natural Te. Afterward, Te was rinsed out by admitting 0.5 M HCl for 70 s, followed by three cycles of 2 M HCl for 70 s each. An iterative routine was used to solve the double spike equations using ^{120}Te, ^{124}Te, ^{126}Te and ^{130}Te to derive $\delta^{130}Te/^{126}Te$ results, ^{120}Te, ^{124}Te, ^{126}Te and ^{128}Te to derive $\delta^{128}Te/^{126}Te$ results, and ^{120}Te, ^{124}Te, ^{125}Te, and ^{126}Te to derive $\delta^{125}Te/^{126}Te$ results.[35] Each group of four samples was bracketed with NIST SRM 3156 standard analyses before and after; sample results were normalized to the average Te isotope measurement of this standard over the analytical session.

2.6 Concentration measurement

To estimate the concentration of each sample for accurate spike addition, 0.2 mL of the digested samples were diluted in 2 mL of Milli-Q water to a final matrix of 5% HNO_3 and 0.1% HCl. Samples were measured on an iCAP Q ICP-MS (Thermo Fisher Scientific). The mass ^{125}Te was measured over 5 cycles with a 0.03 second integration time. An internal standard, consisting of ^{115}In, was mixed with the sample via an inline addition to correct for instrumental drift and matrix effects. The limit of detection was 0.02 ng mL^{-1} Te and the limit of quantification was 0.31 ng mL^{-1}.

Isotope dilution was used to obtain more precise concentrations [36]. The double spike data reduction calculations yield a highly precise determination of the spike:sample ratio, allowing calculating of the sample concentration if the double spike concentration is known.

3. Results and Discussion

3.1 Sensitivity and memory

Measurement of Te isotope ratios of natural sediments requires a high-sensitivity measurement method. Average soils contain typically <5 to 100 ng g^{-1} Te.[44] Accordingly, it is very helpful if precise measurements of soils samples can be obtained using less than 10 ng Te per analysis. Sensitivity during the course of this study was on average 600 mV for ^{130}Te for a 1 ng mL^{-1} Te solution, which for a 1.0 mL min^{-1} uptake rate, delivers 1.0 ng min^{-1}. This sensitivity arises from the high efficiency of the hydride generation system in delivering Te to the plasma. Although the sample uptake rate is high, the relatively short analysis time of 3.5 minutes permits precise measurement on relatively small sample masses. While Brennecka et al.[38] reported high efficiency using hydride generation to measure Te isotope ratios of calcium-aluminum-rich inclusions (~10 ng used per analysis), that method was designed to measure ^{126}Te anomalies in meteorites using internal normalization. The present study is the first to combine the double-spike technique with hydride generation to measure mass-dependent fractionation.

Surprisingly, our measurements on our instrument using desolvating nebulization (Aridus II system) yielded similar Te beam intensity at the same rate of Te mass consumed per unit time. This is an important result as hydride generation has been considered to produce superior sensitivity relative to the desolvating nebulizer for certain hydride forming elements like Sb and Se due to the efficiency of hydride formation and transfer into the mass spectrometer. The hydride sample introduction system used in this study produced equivalent sensitivity to that of Fehr et al.[20] and Fukami et al.[21]. However, the Nu Plasma HR instrument used in this study was manufactured in 2004; newer MC-ICP-MS instruments would probably afford at least 2 times greater sensitivity.

There are significant advantages and disadvantages to each sample introduction system. As reported by Brennecka et al.,[38] at times we observed significant precipitation of elemental Te inside the hydride generation system. This caused slow wash-out of Te memory in the hydride generation system between samples and a decrease in sensitivity. Keeping the sample concentration below 5 ng mL^{-1} Te and tuning the instrument using a 0.5 ng mL^{-1} Te solution helped limit memory effects. We also avoided continuous measurement longer than 4 minutes and rinsed immediately after each analysis with a 0.5 M HCl wash followed by three 2 M HCl washes. In addition, while the Sn contribution from the $NaBH_4$ is significant

for hydride generation (^{118}Sn ~30 to 100 mV), it will be corrected by on-peak zeroes and by monitoring ^{118}Sn.

A positive aspect of hydride generation is the avoidance of certain interferences that do not form hydrides. For example, barium (Ba) is an isobaric interference on ^{130}Te (0.11%) and ^{132}Xe (0.10%), which was monitored to correct for Xe on ^{126}Te, ^{128}Te, and ^{130}Te. This is a complex interference to correct for, due to the simultaneous impacts on ^{130}Te and the Xe correction. Ba would need to be reduced to very low levels by ion exchange chromatography or corrected for by monitoring ^{135}Ba, which is not feasible in our current detector setup. Furthermore, if solutions contain a simple matrix and low Sn (e.g. experimental samples), Te isotope measurements can be made by hydride generation with minimal preparation. This is in contrast to the DSN, where all analytes are transported into the mass spectrometer and could cause matrix or isobaric interferences.

In addition, the H_2 passed to the plasma by the hydride generation system suppresses the intensity of Xe and the Ar trimer, an impurity in Ar gas, thus decreasing the impact of these interferences. Furthermore, hydride generation also decreases the impact of Sn in sample solutions, as most Sn is not delivered to the plasma: Optimal stannane (SnH_4) generation requires basic conditions very different from those used for H_2Te generation.[45]

The sensitivity of both sample introduction methods allows for determination of rocks with average crustal Te concentrations. Samples containing more than 15 ng g^{-1} Te can be analyzed using the purification methods in this study. This range is relevant to natural sediments with lower Te content, such as CLG-1 and CLRD-3.0, and mafic rocks[35, 46]. For Te concentrations less than 15 ng g^{-1}, where more than 0.5 g of sample is required, δ^{130}Te/^{126}Te can be measured using separations of a single spiked sample split among parallel columns to distribute the matrix load. There will be a higher blank in the recombined sample. However, it will be considerably less than twice our current procedural blank, as the contribution of the blank is only from a few additional sources (column, column frit, and resin). This procedure may be suitable for average crustal rocks with lower Te contents, such as granites[46].

3.2 Precision and secondary standards

Long-term δ^{130}Te/^{126}Te reproducibility was assessed as twice the standard deviation (2σ) of repeated analyses over 2 years. Precision for NIST SRM 3156 processed through the

sample preparation steps was ±0.06‰ (2σ) and 0.10‰ (2σ)for 100 ng (n = 11) and 50 ng (n=5) aliquots, respectively. For repeat analyses of a single bottle of the dissolved Alfa Aesar Te(VI) powdered standard (n= 39) our uncertainty was ±0.09‰ (2σ) for $\delta^{130}Te/^{126}Te$ (Table 2). The average $\delta^{130}Te/^{126}Te$ of the bracketing standard, NIST SRM 3156, was on average 0.04 ± 0.09‰ (2σ) (n=71). Average internal precision for $\delta^{130}Te/^{126}Te$, $\delta^{128}Te/^{126}Te$, and $\delta^{125}Te/^{126}Te$ was 0.07‰, 0.05‰ and 0.05‰ (2σ), respectively.

The long-term average $\delta^{130}Te/^{126}Te$ of the Te(VI) reagent used as an in-house standard was 0.84 ± 0.09‰ (2σ) relative to NIST SRM 3156. The Te(IV) Alfa Aesar reagent used as a second in-house standard was isotopically identical to NIST SRM 3156 within uncertainty. The offsets between these standards and NIST SRM 3156 were useful as secondary checks on analysis quality.

Repeat analyses of the Alfa Aesar Te(VI) solution were made at varying intensities to examine the impact on precision. When ^{130}Te intensity was less than 0.8V, $\delta^{130}Te/^{126}Te$ and $\delta^{128}Te/^{126}Te$ values were measured outside of the accepted range of uncertainty and doubled for every factor of two decrease in intensity (Figure 1). This is equivalent to ~1.25 ng mL^{-1} Te for average instrument conditions. The increase in measured $\delta^{130}Te/^{126}Te$, $\delta^{128}Te/^{126}Te$, and $\delta^{125}Te/^{126}Te$ variability at lower Te intensities is due to an increasing impact of background interferences, such as ^{120}Sn and ^{124}Sn, and counting statistics-related noise on the measurement.

Overall, replicate measurements of natural samples (Table 3) show similar precision to that of the standards, implying good reproducibility of the digestion and ion exchange purification procedures. Higher variability in repeated measurements of Nod-P-1 (2σ: 0.12‰) and MAG-1 (2σ: 0.15‰) may reflect some heterogeneity within the powdered samples, as has been suggested by Fukami et al.[21] for their analyses of ferromanganese nodules. For samples yielding less than 8 ng of Te or ^{130}Te less than 1.2 V, $\delta^{130}Te/^{126}Te$, $\delta^{128}Te/^{126}Te$, and $\delta^{125}Te/^{126}Te$ could be obtained with the trade-off of less precise measurements (Figure 1).

Our $\delta^{130}Te/^{126}Te$ measurement uncertainty (Table 2) is somewhat greater than the reported uncertainties of the most precise previously published methods[20, 21]; this difference arises from the current amplifier configuration of our instrument. A careful baseline analysis revealed no contributions from interferences other than ^{130}Xe, and because our Xe correction

is both small and effective (see below), the added uncertainty cannot be attributed to interferences. Rather, some of our reported uncertainty arises from our use of a 10^{10} Ω resistor in the pre-amplifier for the collector used to measure ^{130}Te. Baseline (Johnson-Nyquist) noise measurements were 4 times higher on this collector than the others, which have 10^{11} Ω resistors. The resulting increase in uncertainty can be determined by calculating baseline noise on this channel (taking into account the total time of integration), multiplying by ¾ (¾ of the noise is excess noise cause by the use of the 10^{10} Ω resistor), and propagating this error through the isotope ratio measurement and double spike calculations. When the effect of the excess noise is removed, reproducibility of the standards and natural materials is about equal to that reported in Fehr et al.[31]. Accordingly, this method is expected to afford ±0.06‰ precision (2σ) on δ^{130}Te/^{126}Te for instruments with standard 10^{11} Ω resistors.

3.3 ^{120}Te-^{124}Te Double Spike

A spike to sample molar ratio of 0.98 was determined to be optimal for the inversion isotopes ^{130}Te, ^{126}Te, ^{124}Te, and ^{120}Te. This was based on repeated measurements of standards spiked with different proportions of spike, to minimize uncertainties in the final δ^{130}Te/^{126}Te associated with the spike composition. At this spike to sample composition, the precision observed is similar to the model generated by the Double Spike Toolbox[43] (Figure 2). The accuracy of the spike composition was assessed by repeated measurements of lower (DS/natural ~ 0.60) and higher (DS/natural ~ 2) spiked samples (Figure 2). No statistically significant offsets were observed for δ^{130}Te/^{126}Te, δ^{128}Te/^{126}Te, and δ^{125}Te/^{126}Te (Table 2). The reproducibility of the lower- and higher-spiked standards were ±0.08‰ and ±0.09‰, respectively, similar to the precision of the normally spiked sample (Table 2). The optimal molar spike to sample ratio is noticeably higher than that recommended by the Double Spike Toolbox (DS/natural~ 0.62).[43] However, the Double Spike Toolbox does not take into account effects of interferences. We find that increasing the spike to sample ratio lessens the influence of ^{120}Sn- and ^{124}Sn-related on the two spike isotopes leading to smaller errors on δ^{130}Te/^{126}Te, δ^{128}Te/^{126}Te, and δ^{125}Te/^{126}Te and overall better precision.

3.4 Effectiveness of Te purification methods, and blank results

Given the low abundance of Te compared to Sn (an isobaric interference) and Fe (a suppressant of hydride formation) in many terrestrial samples, separation from these interferences is challenging, yet important. To demonstrate effective Te separation from Sn- and Fe-rich samples, we present elution curves of a Nod-P-1 digestion (Figure 3) focusing on potential hydride-forming interferences and Fe. Arsenic, Se, and Fe are known suppressants of Te hydride formation at moderate concentrations, while Sn and Sb are isobaric interferences.[47] Yields for Te in Nod-P-1 (0.05 g digested) were high, and we achieve effective separation of Te from interfering matrix elements (Table 1). Elution with 8 mL of 1 M HNO_3 resulted in full recovery of Te (101.6%) similar to the results of the "HCl method" in Fehr et al.[37] and Wang and Becker[23] using a 3 mL AG1-X8 anion exchange column. The 5 M HF step eluted 69% of the total Fe while ~30% of the Fe was retained on the column (Figure 3A). Approximately 563 ng (<0.1%) of Fe were eluted with the Te fraction (1 M HNO_3). Selenium and other sample matrix elements were removed during the sample-loading step and the rinse with 6 M HCl. Antimony was mostly (>91%) retained on the column, presumably as $SbCl_6^-$, which adsorbs strongly in acidic conditions on basic resin.[48] In the 1 M HNO_3 elution, 124 ng of Sb was eluted (2.5% of the Sb in the digested sample) as $SbCl_6^-$. Approximately 25% of Sn was eluted during the 5 M HF and 2 M HCl steps. Arsenic was also strongly retained in the column, with the exception of the 6 M HCl rinse. In 6 M HCl, most Sn loaded onto the anion-exchange resin is dissolved as $SnCl_5^-$ or $SnCl_4$[48] and was retained during this rinse. In 2 M HCl, Sn(IV) elutes more readily as a neutrally charged species. In 5 M HF, Sn(IV) is moderately adsorbed, which accounts for the partial elution of Sn during this step. The rest was eluted with Te and was separated later (see below).

In the second ion exchange step (cation resin) modified after Wang et al.[39], the first three milliliters of collected fluid contained all recoverable Te (Figure 3B). Sn(IV) hydrolyzes in low molarity acids to form weakly positive ions[49]. Dissolved Sn(IV) in low HCl molarity adsorbed on the acidic resin and, as expected, was not eluted in the collected Te fraction.[48] The residual Fe that was not removed by the anion exchange step was adsorbed on the resin and not eluted with the Te fraction. Sb(V) was eluted with the collected Te fraction. For samples with relatively high Sn/Te (> 38), Sn was not completely separated. The reason behind this is unclear, but may be due to small amounts of dissolved $SnCl_5^-$ or $SnCl_6$ remaining in the sample. Passing the 0.1 M HCl sample solution through a column with 1 mL

AG1-X8 (100-200 mesh) resin removed the remaining Sn[39]. Dissolved Sn(IV) was only eluted at higher molarities of HCl.[39]

Digestion blanks (n=3) were less than 0.01 ng on average. Cumulative blanks for the first two columns were 0.05 ng Te on average (n = 17) and for the third were 0.03 ng Te (n=4). Total cumulative blanks from all three columns are 0.5% of the lowest samples measured using this method. NIST SRM 3156 standards containing 100, 50, 15 ng Te processed through the columns showed no offset relative to unprocessed solutions, indicating that isotopic fractionation either did not occur during the process or was corrected for by the double spike (Table 2).

3.5. Interferences

Correction for Sn-based interferences is essential, as ^{120}Sn (32.58%) and ^{124}Sn (5.79%) are isobaric interferences on both Te spike isotopes, as we observed 30 to 100 mV of ^{118}Sn in the blank during hydride generation measurements. This contribution of Sn is mostly subtracted during on-peak zeros even when the $NaHB_4$ contains relatively high Sn (^{118}Sn > 80 mV). However, on-peak zero subtraction cannot correct for errors arising from incomplete removal of Sn from samples during sample preparation. Doping experiments show that measuring ^{118}Sn (24.22%) and subtracting calculated ^{120}Sn and ^{124}Sn results in an effective correction up to ^{120}Sn/^{120}Te~0.02, equivalent to a 19‰ correction on δ^{130}Te/^{126}Te (Figure 4). This is a high tolerance for Sn, equal to 5 ng mL^{-1} Sn in a 2.5 ng mL^{-1} Te sample with normal spike to sample ratio. An example of high Sn/Te in a natural sample is the standard reference material MAG-1 (Sn/Te~ 54.5). For a required mass of 10 ng Te, approximately 99% of Sn would need to be separated from the purified Te to meet the Sn correction threshold for our initial correction. Given the efficacy of the column procedure in removing Sn, this requirement is not difficult to achieve. Standards did not exceed a ^{118}Sn intensity of 10 mV and did not require column purification.

Above ^{120}Sn/^{120}Te~0.02, we noted that increased Sn doping caused δ^{130}Te/^{126}Te to decrease linearly (Figure 4). This error is most likely caused by fractionation of Sn isotopes in the hydride generation system, which we expect is strong as Sn(IV) undergoes reduction by $NaBH_4$ and is incompletely released. Accordingly, our correction scheme, which assumes Sn of "average natural" composition and the same mass bias as Te, becomes inaccurate. We

do not include a correction for SnH^+ signals, and thus contribution of $^{117}SnH^+$ to ^{118}Sn or $^{119}SnH^+$ to ^{120}Te may be another source of small errors at higher Sn/Te where the primary correction fails. Based on our Sn doping experiments, we suggest a secondary linear correction may be helpful up to $^{120}Sn/^{120}Te$~0.3, the range of $^{120}Sn/^{120}Te$ we examined (Figure 4). We also note that the impact of Sn interferences can be reduced if the molarity of HCl in all samples is within ± 0.1 M of the 4 M HCl acid used for the blank. Discrepancies in HCl molarity in the blank and sample can lead to post-correction excesses in the net Sn signal as the production of stannane during hydride generation is favorable at more basic conditions.[45] Therefore, the HCl molarity of a small aliquot of each sample was checked via titration.

Residual Xe after subtraction of on-peak zeros was corrected successfully using ^{132}Xe measurements. As an impurity in the Ar gas, ^{132}Xe typically varies between 5-15 mV before the correction from one session to another and is stable over the measurement run. While Xe isotopes impact ^{130}Te (^{130}Xe: 4.071%), ^{128}Te (^{128}Xe: 1.910%), ^{126}Te (^{126}Xe: 0.089%), and ^{124}Te (^{124}Xe: 0.095%), this correction is at most ± 0.1‰ on $\delta^{130}Te/^{126}Te$ and is even lower on the other impacted Te isotope ratios. On average, residual ^{130}Xe is 10^{-4} V, as most of the Xe was corrected in the on-peak zero subtraction. As such, it is not a challenging interference to correct for, but could be if Xe concentrations were larger or fluctuated significantly during analyses. For example, high impurities in Ar, as a result of the fractional distillation of air, could possibly cause problematic intensities of isotopically fractionated Xe.

The impact of Te hydrides ($^{124}Te^1H$, $^{125}Te^1H$) was also minimized due to our corrections. Based on measurements of mass 131 while measuring a Te standard solution, we estimate the $TeH^+/Te \sim 10^{-4}$. This magnitude of hydride formation is similar to that of SeH^+/Se in the hydride generation system used here. This value is refined before every run and does not vary by more than ± 3 $x10^{-5}$ between measurement sessions. It is imperative that the double spike is well characterized before this correction is applied, as the TeH^+/Te is tuned using the results of overspiked or underspiked standards at the beginning of each analytical session (see methods section).

While Sb does not directly cause an interference on any isotopes of interest, $^{123}Sb^1H$ could potentially affect ^{124}Te. Figure 5 indicates that this is not consequential at even relatively high Sb added into the standard. Assuming a similar hydride formation rate as

TeH^+/Te of 10^{-4}, a $^{123}Sb/^{130}Te$ ratio of 1.24 would cause a 0.12‰ shift on $\delta^{130}Te/^{126}Te$. This is not apparent in the measurement results given in Figure 5, indicating Sb must have lower rates of hydride formation than noted here for TeH^+/Te. In addition, H_3Sb generation is inefficient when Sb is present in the oxidized Sb(V) form[47], as expected for samples stored in contact with air. As a result, Sb/Te for natural samples measured to date has always been less than that of the maximum Sb doped standard in Figure 5. A $^{123}XH^+/^{124}Te$ correction of 0.00001, nevertheless, is included in our routine in the event of higher Sb intensities.

3.6 Concentration measurements

Concentrations of Nod-P-1, SCO-1, MAG-1, and SGR-1 calculated by isotope dilution overall agree with previously published data (Table 3).[20, 21, 23, 46, 50] The average of multiple digestions of Nod-P-1 is identical to all three previous reported results, within the uncertainties. SCO-1 and MAG-1 agree within uncertainty with concentration values in Wang et al.[23]. Variability over multiple measurements could be the result of heterogeneity in the powdered material or contribution of error from weighing errors inherent in measuring small sample masses (e.g., 0.02 mg) using the balance available in our laboratory. Our isotope dilution results for USGS soils and mine tailings provide more precise concentration measurements than previous measurements by single-collector ICP-MS digestions. While there are no previously published concentrations of CLRD-3.0 and CLG-1, good reproducibility indicates nearly full recovery of samples.

3.7. Isotope measurements of natural samples

The NIST SRM 3156 standard solution used to define the zero point on the delta scale originates from the same batch (Lot: 140830) measured in Fukami et al.[21], Therefore, we can compare directly our results to values of Nod-P-1 reported in this study. The NIST SRM 3156 measured by Fehr et al.[20] is sourced from a different lot, which, in this case, originates from separate materials and manufacturers and cannot be directly compared. Nevertheless, a few of our values match well with those published in Fehr et al.[20] and could be indicative of similar isotopic compositions between lots. Our average Nod-P-1 agrees with those of both Fehr et al.[20] and Fukami et al.[21] highlighting the relative uniformity in this specific powdered material despite possible chemical heterogeneity in the original nodules

and in other samples (see below). The average of MAG-1 measured in our study overlaps within analytical uncertainty to values in Fehr et al.[20]. However, our average $\delta^{130}Te/^{125}Te$ for SGR-1 is significantly greater than the single measurement reported for the same reference material in Fehr et al.[20]. This may be due to either differences in the $\delta^{130}Te/^{125}Te$ NIST SRM 3156 or heterogeneity in the sample bottle. Variability in selenium isotope ratios has been noted before between different bottles of SGR-1, suggesting that this material may be isotopically heterogeneous.[51]

All samples measured were isotopically heavier than NIST SRM 3156; the heaviest and lightest being the Vulcan Yellow Precipitate (1.29 ± 0.08 ‰) and C350500 (0.08 ± 0.06 ‰), respectively. This is the largest range in $\delta^{130}Te/^{126}Te$, $\delta^{128}Te/^{126}Te$, and $\delta^{125}Te/^{126}Te$ observed in low-temperature environments yet, suggesting that Te stable isotopes fractionate during low-temperature processes in marine and terrestrial weathering environments. Redox reactions may contribute to the observed isotopic fractionation. For example, Fukami et al.[21] suggested that oxidation of Te(IV) to Te(VI) in ferromanganese crust may result in isotopically heavy values. Reduction of Te oxyanions to elemental Te(0) in reducing soils may also drive the residual Te isotopically heavier as well, as has been shown for various abiotic reductants[11]. Alternatively, the major fractionating pathway could be adsorption, as both Te(VI) and Te(IV) adsorb strongly on iron oxides.[10] As observed for W adsorption on ferrihydrite, adsorption of metal oxyanions results in an isotopically lighter sorbent relative to the original fluid due to differences in the coordination environment.[52] As the magnitude of adsorption increases, the solid sample could evolve to a heavier Te isotopic composition. This is another interpretation for the correlation between the higher Te/Se ratio and $\delta^{130}Te/^{125}Te$ as noted in Fukami et al. (2018). It also may explain why certain samples, that have undergone a greater extent of oxidation or contain greater Fe_2O_3%, like the Vulcan Yellow precipitate, seem to be isotopically heavier than less Fe_2O_3% rich samples. For example Nod-P-1 is 0.35‰ heavier than the marine mud, MAG-1 and topsoil, C320293, is 0.25‰ greater than the Horizon A soil, C350500.

Te isotope studies have not yet found evidence of mass-independent fractionation of Te isotopes in terrestrial samples[20, 22, 53], despite significant nuclear field shift effects on Te isotopes observed in a laboratory study[54]. When comparing $\delta^{128}Te/^{126}Te$ and $\delta^{125}Te/^{126}Te$ to $\delta^{130}Te/^{126}Te$, we observe no significant deviations from mass-dependent fractionation in the

Alfa Aesar Te(VI) powder standards (Figure 6). We also see no deviation within analytical uncertainty from an exponential mass-dependent fractionation relationship in the natural samples either (Figure 6). With additional replicate analyses leading to higher precision, mass-independent fractionation may be resolved. Assuming an exponential mass-dependent kinetic isotope fractionation law, the slope (β) of the relationships in Figure 6 is expressed as:

$$\beta = \frac{ln\frac{m_{126}}{m_x}}{ln\frac{m_{126}}{m_{130}}},$$

where X is either the mass of ^{128}Te or ^{125}Te. This observation does not preclude the possibility of mass-independent fractionation in the future though. The fact that mass-dependent patterns were always observed provide further evidence of the fidelity of the measurements despite several interferences. In particular, the Sn correction is effective over a large range of Sn/Te in the samples. Improper removal of Sn to produce a large Sn excess would not only artificially depress the δ^{130}Te/^{126}Te and δ^{128}Te/^{126}Te, and increase δ^{125}Te/^{126}Te, but also affect mass-independent fractionation due to the $^{124}TeH^+$ correction on ^{125}Te.

4. Conclusions

The methods detailed in this study provide a new approach to measure Te isotopes.

- While we expected that the hydride generation method would allow for measurements on lower masses of Te with better ionization efficiency, under the current conditions on our instrument, we observe that the sensitivity of the hydride generation sample introduction is similar to that achieved with a desolvating nebulizer (Aridus II; <8.75 ng Te per measurement).
- Hydride generation avoids the introduction of certain interfering elements like Ba, which can be complicated to correct for. Furthermore, many solutions containing low dissolved Sn and Fe concentrations can be analyzed without any matrix separation. This enables a large savings in time for some sample types with simple matrices, such as those generated by laboratory experiments and possibly high-Te contaminated water.
- The attainable precision of this method using about 8 ng per measurement (2σ~ 0.09‰ for δ^{130}Te/^{126}Te) is similar to that of previously published methods.

- The large range in $\delta^{130}Te/^{126}Te$ (1.21‰) of several natural samples presented here indicates that isotopic fractionation of Te is prevalent in low-temperature marine and terrestrial environments.
- Despite the potential for effects from interferences like Sb, Sn and Fe, the ion exchange procedure we modified from previous methods effectively purifies Te from the sample matrix. Future studies can apply this method to Te isotope measurements of natural waters.
- We observed that the $\delta^{130}Te/^{126}Te$, $\delta^{128}Te/^{126}Te$, and $\delta^{125}Te/^{126}Te$ results for reagent Te and the natural samples follow mass-dependent fractionation as has been observed in all studies to date.

Although laboratories using desolvating nebulization should be able to achieve high-quality measurements with similar masses of Te, we suggest that future laboratory and field studies can use this hydride generation approach advantageously due to its ability decrease or eliminate interferences and matrix-related problems.

Conflicts of interest

There are no conflicts to declare.

Acknowledgements

We thank Dr. Sarah Hayes (USGS) for supplying the mine tailing samples, Dr. David Smith (USGS) for providing the USGS soil samples, Professor Noah Planavsky for supplying samples CLG-1 and CLRD-3.0 and Professor Craig Lundstrom (UIUC) for contributing the USGS standard reference materials. In addition, we would like to acknowledge help from the late Dr. Thomas Bullen (USGS), who provided the ^{120}Te and ^{124}Te spike solutions from a source unknown to the authors.

This material is based upon work supported by the National Science Foundation under Grant No. NSF EAR 16-60

Tables

Table 1. Detector setup showing associated Te isotopes and isobaric interferences.

L4	L3	L1	Ax	H1	H2	H3	H4	H5	H6
^{118}Sn	**^{120}Te** ^{120}Sn ^{119}SnH^{+} ^{40}Ar^{40}Ar^{40}Ar	**^{123}Te** ^{123}Sb ^{122}TeH^{+}	**^{124}Te** ^{124}Sn ^{123}SbH^{+} ^{123}TeH^{+} ^{124}Xe	**^{125}Te** ^{125}TeH^{+}	**^{126}Te** ^{126}Xe ^{126}TeH^{+}	^{127}I	**^{128}Te** ^{128}Xe	**^{130}Te** ^{130}Xe ^{130}Ba	^{132}Xe ^{132}Ba

Table 2. $\delta^{130}Te/^{126}Te$ data of standards.

Standard	Number of Analyses	$\delta^{130}Te/^{126}Te$ (‰)	2σ
In-house standard solution from Alfa Aesar Te(VI) powder (lot no. Y05A029)	39	0.84	0.09
In-house standard solution from Alfa Aesar Te(IV) powder (lot no. M27C052)	13	-0.06	0.14
Processed NIST SRM 3156 (100 ng)[a]	11	0.00	0.06
Processed NIST SRM 3156 (50 ng)[a]	5	0.04	0.10
Processed NIST SRM 3156 (15 ng)	1	-0.06	n.d.
Processed NIST SRM 3156 (15 ng)	1	0.00	n.d
NIST SRM 3156 (DS/sample ~0.6)	7	0.00	0.08
NIST SRM 3156 (DS/sample ~ 2)	5	-0.05	0.09
NIST SRM 3156 bracketing standards	71	0.04	0.09

[a.] Processed NIST SRM 3156 standards represent an aliquot of standard run through all three columns (Section 2.3).

Table 3. Results of Te concentrations and Te isotope ratios of natural samples.[a]

Sample	Te [μg g^{-1}]	2σ	$\delta^{130}Te/^{126}Te$ (‰)	2σ	$\delta^{128}Te/^{126}Te$ (‰)	2σ	$\delta^{125}Te/^{126}Te$ (‰)	2σ	$\delta^{130}Te/^{125}Te$ (‰)	2σ
Nod-P-1										
This study	4.70		0.50		0.20		-0.22		0.72	
This study	5.44		0.44		0.25		-0.12		0.66	
This study	4.59		0.59		0.33		-0.09		0.68	
This study	4.58		0.51		0.22		-0.07		0.59	
This study	5.08		0.45		0.27		-0.07		0.52	
Average	**4.88**	**0.75**	**0.50**	**0.12**	**0.25**	**0.10**	**-0.11**	**0.12**	**0.64**	**0.16**
Fehr et al. (2018)	n.d.								0.54	0.12
Fukami et al. (2018)	5.14	0.31							0.66	0.05
Axelsson et al.(2002)	4.80	0.40								
Schirmer et al. (2014)	4.95	0.40								
SCO-1										
This study	0.08		0.12		0.06		0.02		0.09	
This study	0.08		0.13		0.04		0.01		0.12	
Average	**0.08**	**0.00**	**0.13**	**0.02**	**0.05**	**0.03**	**0.01**	**0.01**	**0.10**	**0.03**
Wang et al. (2014)	0.07	0.02								
Schirmer et al. (2014)	0.09	0.01								
SGR-1										
This study	0.25		0.32		0.29		-0.13		0.46	
This study	0.25		0.29		0.17		-0.01		0.30	
Average	**0.25**	**0.00**	**0.31**	**0.04**	**0.23**	**0.18**	**-0.07**	**0.16**	**0.31**	**0.23**
Schirmer et al. (2014)	0.24	0.01								
Fehr et al. (2018)	0.20	n.d.							0.04	0.08
MAG-1										
This study	0.07		0.15		0.08		-0.04		0.20	
This study	0.06		0.17		0.24		-0.18		0.33	
This study	0.07		0.05		0.12		-0.09		0.29	
This study	0.06		0.23		0.28		-0.16		0.45	
Average	**0.07**	**0.01**	**0.15**	**0.15**	**0.18**	**0.19**	**-0.12**	**0.13**	**0.32**	**0.21**
Wang et al. (2014)	0.07	0.01								

Sample	Te [µg g^{-1}]	2σ	$\delta^{130}Te/^{126}Te$ (‰)	2σ	$\delta^{128}Te/^{126}Te$ (‰)	2σ	$\delta^{125}Te/^{126}Te$ (‰)	2σ	$\delta^{130}Te/^{125}Te$ (‰)	2σ
Fehr et al. (2018)	0.05	n.d.							0.01	0.10
C320293										
This study	69.94		0.35		0.16		-0.09		0.47	
This study	49.74		0.42		0.14		-0.02		0.46	
This study	56.72		0.33		0.15		-0.07		0.50	
This study	54.69		0.32		0.14		-0.08		0.39	
Average	**57.77**	**17.25**	**0.36**	**0.09**	**0.15**	**0.02**	**-0.07**	**0.06**	**0.46**	**0.09**
USGS	50.50	n.d.								
C350500										
This study	18.34		0.06		0.00		-0.10		0.20	
This study	17.92		0.11		-0.04		-0.07		0.25	
Average	**18.13**	**0.59**	**0.08**	**0.06**	**-0.02**	**0.05**	**-0.08**	**0.05**	**0.23**	**0.07**
USGS	9.60	n.d.								
Masonic surface										
This study	1070.89		0.31		0.09		-0.16		0.49	
This study	1810.83		0.39		0.18		-0.10		0.52	
Average	**1440.86**	**1046.43**	**0.35**	**0.11**	**0.13**	**0.12**	**-0.13**	**0.09**	**0.51**	**0.04**
Vulcan yellow precipitate										
This study	571.75		1.33		0.75		-0.36		1.64	
This study	684.71		1.24		0.66		-0.39		1.50	
This study	604.63		1.28		0.75		-0.30		1.57	
This study	627.46		1.31		0.68		-0.23		1.55	
Average	**622.14**	**95.14**	**1.29**	**0.08**	**0.71**	**0.09**	**-0.32**	**0.14**	**1.57**	**0.12**
Ute Ulay surface										
This study	19.92		0.47		0.21		-0.13		0.60	
This study	17.03		0.46		0.22		-0.12		0.48	
This study	18.03		0.54		0.33		-0.19		0.67	
This study	16.93		0.42		0.34		-0.06		0.52	
Average	**17.98**	**2.77**	**0.47**	**0.09**	**0.27**	**0.14**	**-0.13**	**0.11**	**0.57**	**0.17**
Ute Ulay deep										
This study	1.66		0.36		0.22		-0.13		0.47	

Sample	Te [μg g^{-1}]	2σ	$\delta^{130}Te/^{126}Te$ (‰)	2σ	$\delta^{128}Te/^{126}Te$ (‰)	2σ	$\delta^{125}Te/^{126}Te$ (‰)	2σ	$\delta^{130}Te/^{125}Te$ (‰)	2σ
This study	1.04		0.40		0.24		-0.15		0.55	
This study	1.32		0.40		0.25		-0.12		0.52	
Average	**1.34**	**0.63**	**0.38**	**0.05**	**0.23**	**0.03**	**-0.13**	**0.03**	**0.51**	**0.08**
Delamar big tails surface										
This study	233.67		0.31		0.20		-0.02		0.35	
This study	337.01		0.41		0.20		-0.08		0.48	
This study	335.40		0.31		0.27		-0.10		0.41	
Average	**302.03**	**118.41**	**0.34**	**0.11**	**0.22**	**0.08**	**-0.07**	**0.08**	**0.41**	**0.14**
CLRD-3.0										
This study	0.037		0.32		0.09		-0.02		0.34	
This study	0.041		0.40		0.21		-0.13		0.53	
Average	**0.039**	**0.007**	**0.36**	**0.11**	**0.15**	**0.16**	**-0.08**	**0.16**	**0.44**	**0.27**
CLG-1										
This study	0.020		0.14		0.08		0.00		0.14	
This study	0.018		0.08		0.04		-0.11		0.19	
Average	**0.019**	**0.003**	**0.11**	**0.08**	**0.06**	**0.05**	**-0.05**	**0.15**	**0.17**	**0.07**

[a]All values reported for this study represent samples digested, purified, and measured once. *Fehr et al.[20] and Fukami et al.[21] values are compared to the average NIST SRM 3156 values reported in their respective studies. $\delta^{130}Te/^{125}Te$ results are calculated using ^{120}Te, ^{124}Te, ^{125}Te, and ^{130}Te as the inversion isotopes.

Figures

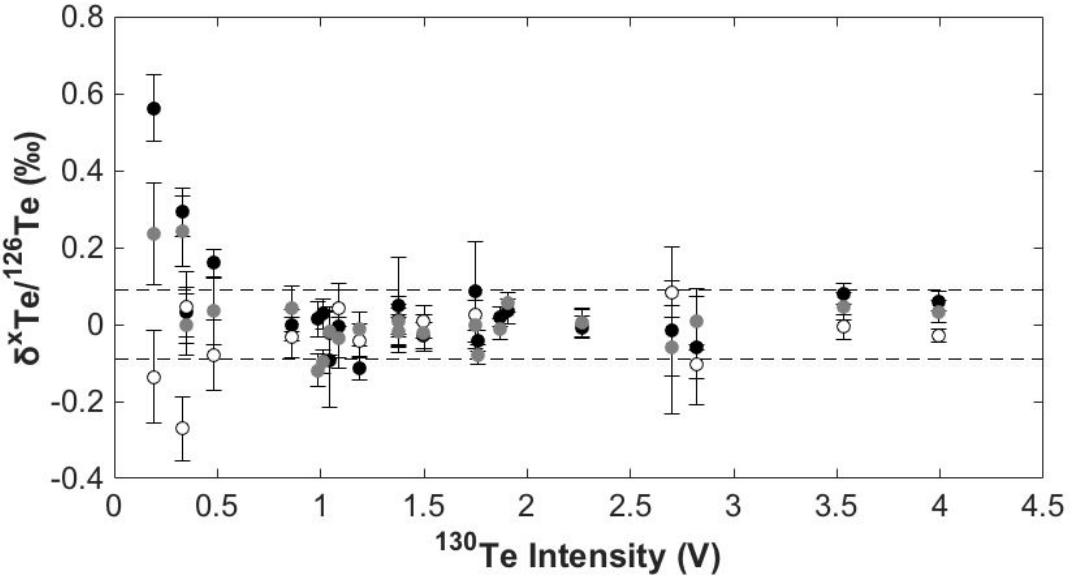

Figure 1. Repeated analyses of $\delta^{130}Te/^{126}Te$ (black circles), $\delta^{128}Te/^{126}Te$ (grey circles), or $\delta^{125}Te/^{126}Te$ (open circles) at varying intensities of the Alfa Aesar Te(VI) in-house standard with optimal spike:sample ratio normalized to the average value of a 2.5 ppb solution of Alfa Aesar Te(VI). The dashed band denotes the average envelope of uncertainty (2σ) for $\delta^{130}Te/^{126}Te$. Error bars represent twice the standard error of an individual analysis.

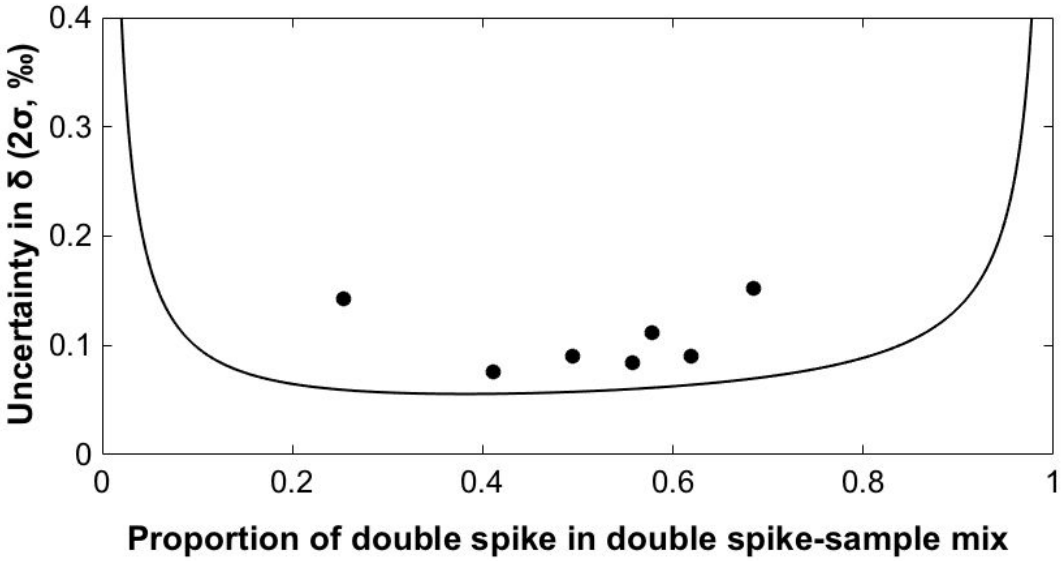

Figure 2. Uncertainties of $\delta^{130}Te/^{126}Te$ over various proportions of double spike in the double spike-sample mixture. Black circles represent triplicate measurements of NIST SRM 3156 at different proportion of double spike in the double spike-sample mixture (molar basis). The solid line denotes the error propagation model by Rudge et al.[43] using the double spike composition from this study, where the optimal proportion of double spike in the double spike mixture is 0.28.

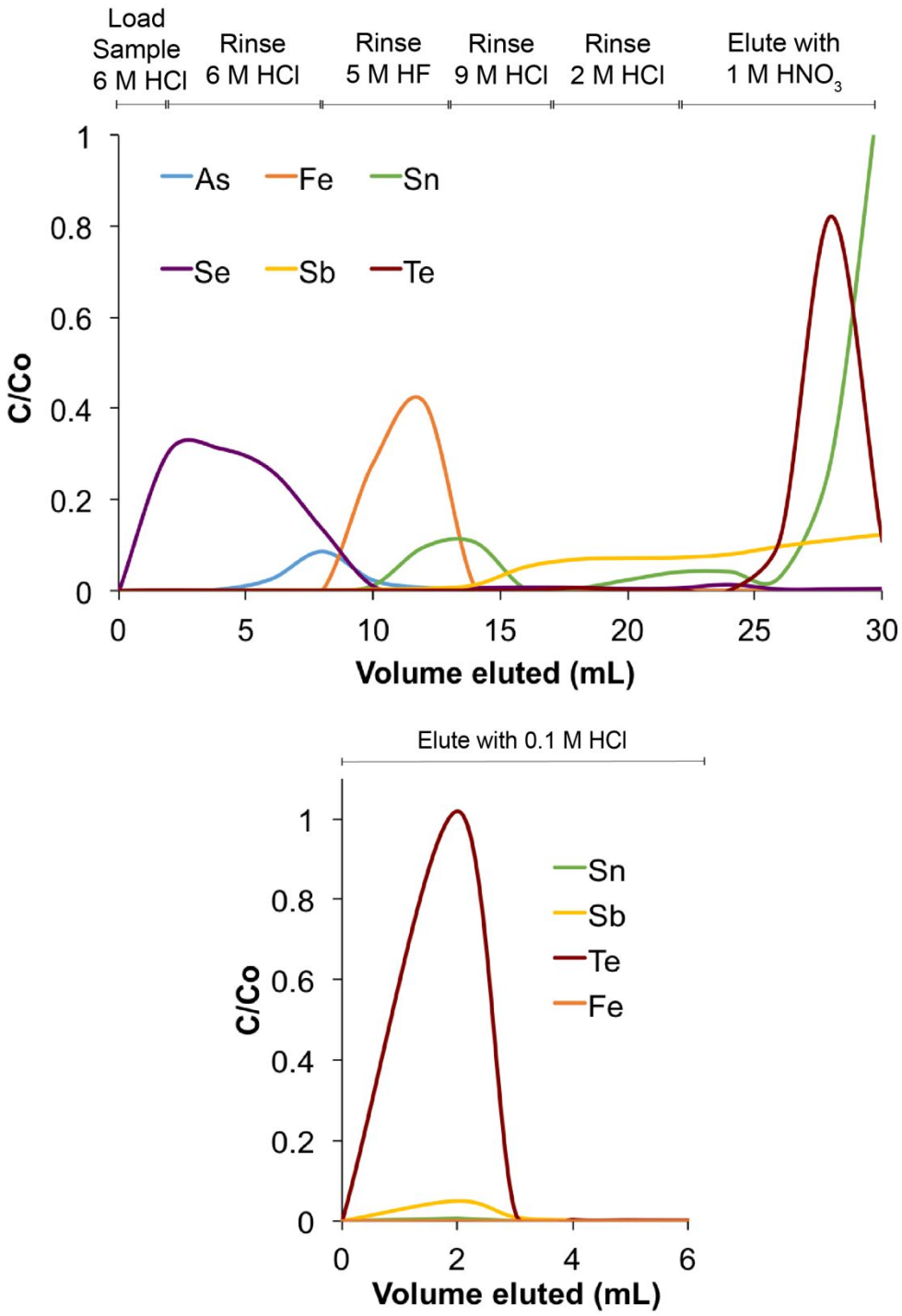

Figure 3. (A) Elution curves for a digestion of 50 mg of SRM Nod-P-1 following a modified anion exchange procedure from Fehr et al. (2004) and Wang and Becker (2014). (B) Elution curves for the secondary column to separate Sn and Fe from Te using AG 50W-X8 cation-exchange resin. C/Co is defined as the elemental mass eluted over the total elemental mass of sample loaded into the column.

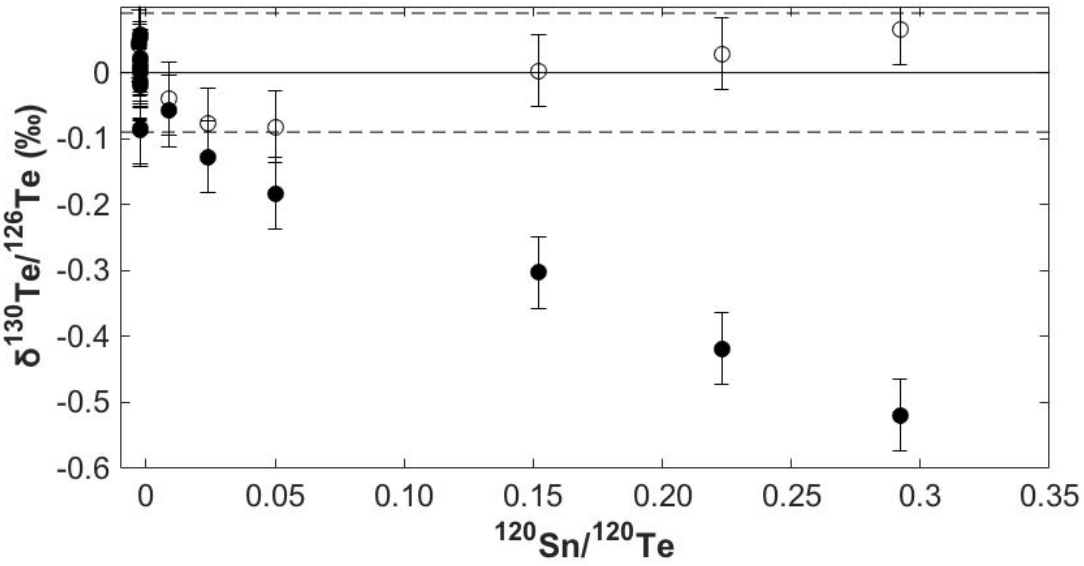

Figure 4. $\delta^{130}Te/^{126}Te$ with increasing amounts of Sn doped into the standard Alfa Aesar Te(VI) solution and normalized to the average Alfa Aesar Te(VI) value. Filled circles show measured values that are corrected with the primary correction. Open circles have a secondary correction based on a linear fit between $\delta^{130}Te/^{126}Te$ and Sn/Te. These corrected values fall within the average envelope of uncertainty (2σ) for repeated analyses of Alfa Aesar Te(VI) denoted by the dashed lines. Error bars are twice the average standard error of the measurements.

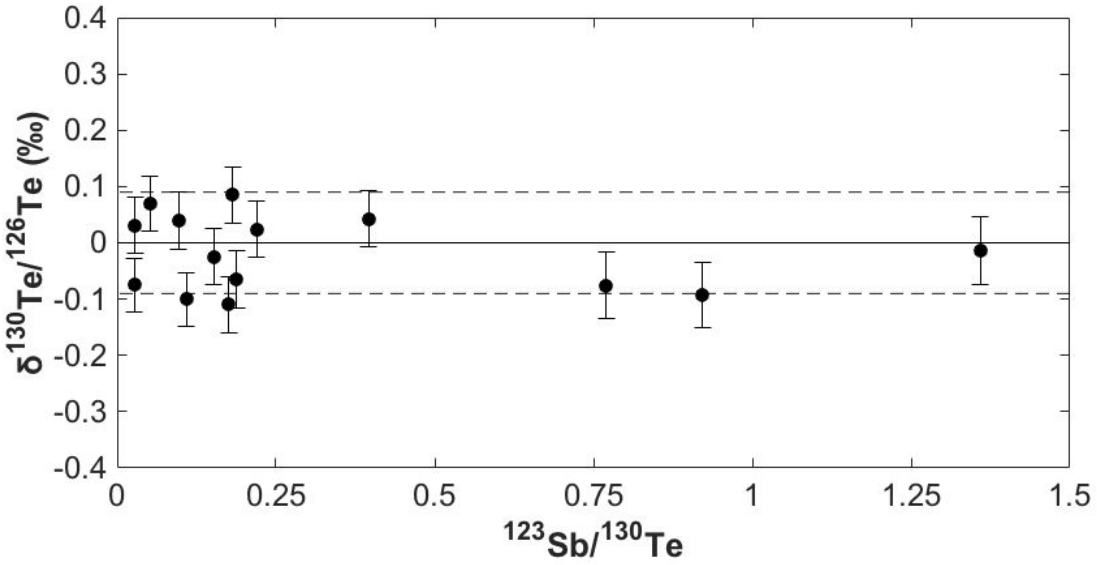

Figure 5. $\delta^{130}Te/^{126}Te$ with increasing amounts of Sb added to the standard NIST SRM 3156, as indicated by the ratio of ^{123}Sb to ^{130}Te on the x axis. No $^{123}SbH^+$ correction is applied to the data shown. The impact of $^{123}SbH^+$ on measurement of ^{124}Te is negligible for $^{123}Sb/^{130}Te < 1.4$. The dashed lines indicate the average envelope of uncertainty (2σ) for repeated analyses of NIST SRM 3156. Error bars are twice the standard error of each measurements.

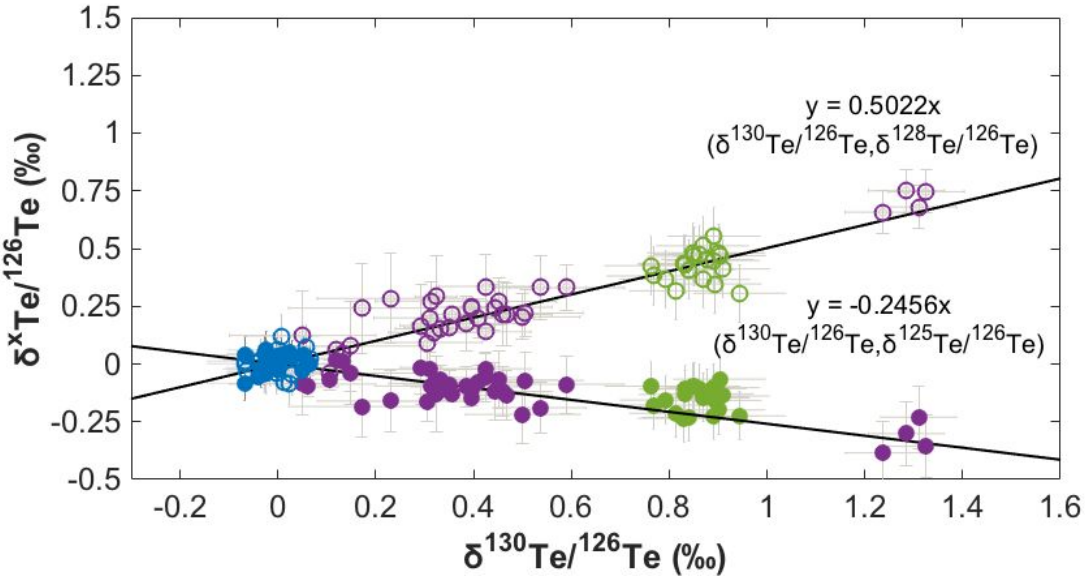

Figure 6. Comparison of $\delta^{128}Te/^{126}Te$ or $\delta^{125}Te/^{126}Te$ by $\delta^{130}Te/^{126}Te$. Open symbols reflect the ($\delta^{130}Te/^{126}Te$, $\delta^{128}Te/^{126}Te$) correlation, while closed symbols show ($\delta^{130}Te/^{126}Te$, $\delta^{128}Te/^{126}Te$). All symbols fall within analytical uncertainty (2σ, grey error bars) of the expected relationship ($\delta^{128}Te/^{126}Te = 0.5022 \times \delta^{130}Te/^{126}Te$ and $\delta^{125}Te/^{126}Te = -0.2456 \times \delta^{130}Te/^{126}Te$), based on exponential-law, mass-dependent kinetic fractionation. Blue symbols are multiple analyses of NIST SRM 3156; purple symbols reflect natural samples; green symbols are multiple analyses of the Alfa Aesar Te(VI) reagent.

References

1. K. Zweibel, *Science*, 2010, **328**, 699-701.
2. W. T. Perkins, *The Science of the total environment*, 2011, **412-413**, 162-169.
3. R. Goldfarb, *ellurium—The bright future of solar energy*, 2015.
4. M. C. Yarema and S. C. Curry, *Pediatrics*, 2005, **116**, e319-e321.
5. L. Gerhardsson, in *Handbook on the Toxicology of Metals (Fourth Edition)*, eds. G. F. Nordberg, B. A. Fowler and M. Nordberg, Academic Press, San Diego, 2015, DOI: https://doi.org/10.1016/B978-0-444-59453-2.00054-8, pp. 1217-1228.
6. J. R. Hein, A. Koschinsky and A. N. Halliday, *Geochimica et Cosmochimica Acta*, 2003, **67**, 1117-1127.
7. N. Belzile and Y.-W. Chen, *Applied Geochemistry*, 2015, **63**, 83-92.
8. J. R. Hein, A. Koschinsky and A. N. Halliday, *Geochimica et Cosmochimica Acta*, 2003, **67**, 11.
9. D. S. Lee and J. M. Edmond, *Nature*, 1985, **313**, 782-785.
10. H.-B. Qin, Y. Takeichi, H. Nitani, Y. Terada and Y. Takahashi, *Environ. Sci. Technol.*, 2017, **51**, 6027-6035.
11. S. M. Baesman, T. D. Bullen, J. Dewald, D. Zhang, S. Curran, F. S. Islam, T. J. Beveridge and R. S. Oremland, *Appl. Environ. Microbiol.*, 2007, **73**, 2135-2143.
12. D. E. Taylor, *Trends in Microbiology*, 1999, **7**, 111-115.
13. N. J. Planavsky, C. T. Reinhard, X. Wang, D. Thomson, P. McGoldrick, R. H. Rainbird, T. Johnson, W. W. Fischer and T. W. Lyons, *Science*, 2014, **346**, 635.
14. N. J. Planavsky, J. F. Slack, W. F. Cannon, B. O'Connell, T. T. Isson, D. Asael, J. C. Jackson, D. S. Hardisty, T. W. Lyons and A. Bekker, *Chemical Geology*, 2018, **483**, 581-594.
15. D. S. Hardisty, Z. Lu, A. Bekker, C. W. Diamond, B. C. Gill, G. Jiang, L. C. Kah, A. H. Knoll, S. J. Loyd, M. R. Osburn, N. J. Planavsky, C. Wang, X. Zhou and T. W. Lyons, *Earth and Planetary Science Letters*, 2017, **463**, 159-170.
16. A. S. Ellis, T. M. Johnson and T. D. Bullen, *Science*, 2002, **295**, 2060-2062.
17. A. S. Ellis, T. M. Johnson, M. J. Herbel and T. D. Bullen, *Chemical Geology*, 2003, **195**, 119-129.
18. C. J. Bopp, C. C. Lundstrom, T. M. Johnson, R. A. Sanford, P. E. Long and K. H. Williams, *Environmental Science & Technology*, 2010, **44**, 5927-5933.
19. R. M. Smithers and H. R. Krouse, *Can. J. Chem.*, 1968, **46**, 583-591.
20. M. A. Fehr, S. J. Hammond and I. J. Parkinson, *Geochimica et Cosmochimica Acta*, 2018, **222**, 17-33.
21. Y. Fukami, J.-I. Kimura and K. Suzuki, *Journal of Analytical Atomic Spectrometry*, 2018, **33**, 1233-1242.
22. A. P. Fornadel, P. G. Spry, M. A. Haghnegahdar, E. A. Schauble, S. E. Jackson and S. J. Mills, *Geochimica et Cosmochimica Acta*, 2017, **202**, 215-230.
23. Z. Wang and H. Becker, *Geostandards and Geoanalytical Research*, 2014, **38**, 189-209.
24. A. Forrest, R. Kingsley and J.-G. Schilling, *Geostandards and Geoanalytical Research*, 2009, **33**, 261-269.

25. F. J. Flanagan and D. Gottfried, *USGS rock standards; III, Manganese-nodule reference samples USGS-Nod-A-1 and USGS-Nod-P-1*, Report 1155, U.S. Govt. Print Off., 1980.
26. F. J. Flanagan, *Descriptions and analyses of eight new USGS rock standards*, Report 840, 1976.
27. D. B. Smith, W. F. Cannon, L. G. Woodruff, F. Solano and K. J. Ellefsen, *Geochemical and mineralogical maps for soils of the conterminous United States*, Report 2014-1082, Reston, VA, 2014.
28. E. P. CM Tschanz, *Geology of mineral deposits of Lincoln County, Nevada*, Mackay School of Mines, Universtiy of Nevada, Reno, NV, 1970.
29. S. M. Hayes and N. A. Ramos, *Environmental Chemistry*, 2019, **16**, 251-265.
30. C. Smith, *History and Development of the Golden Wonder Mine: 1874 to 2011*, LKA International, 2012.
31. S. J. Sutton and J. B. Maynard, *Canadian Journal of Earth Sciences*, 1993, **30**, 60-76.
32. M. G. Babechuk, N. E. Weimar, I. C. Kleinhanns, S. Eroglu, E. D. Swanner, G. G. Kenny, B. S. Kamber and R. Schoenberg, *Precambrian Research*, 2019, **323**, 126-163.
33. Z. C. H. Gao L.Z., Yin, C. Y., Shi X. Y., Wang Z.Q., Liu T. M. Liu P. J., Tang F. and Song B., *Acta Geoscience Sinica*, 2008, **29**, 366-376.
34. C. Li, N. J. Planavsky, G. D. Love, C. T. Reinhard, D. Hardisty, L. Feng, S. M. Bates, J. Huang, Q. Zhang, X. Chu and T. W. Lyons, *Geochimica et Cosmochimica Acta*, 2015, **150**, 90-105.
35. A. Yierpan, S. König, J. Labidi, T. Kurzawa, M. G. Babechuk and R. Schoenberg, *Geochemistry, Geophysics, Geosystems*, 2018, **19**, 516-533.
36. Y.-W. Chen, A. Alzahrani, T.-L. Deng and N. Belzile, *Analytica Chimica Acta*, 2016, **905**, 42-50.
37. M. A. Fehr, M. Rehkämper and A. N. Halliday, *International Journal of Mass Spectrometry*, 2004, **232**, 83-94.
38. G. A. Brennecka, L. E. Borg, S. J. Romaniello, A. K. Souders, Q. R. Shollenberger, N. E. Marks and M. Wadhwa, *Geochimica et Cosmochimica Acta*, 2017, **201**, 331-344.
39. X. Wang, C. Fitoussi, B. Bourdon and Q. Amet, *Journal of Analytical Atomic Spectrometry*, 2017, **32**, 1009-1019.
40. O. Eugster, F. Tera and G. J. Wasserburg, *Journal of Geophysical Research (1896-1977)*, 1969, **74**, 3897-3908.
41. C. M. Johnson and B. L. Beard, *International Journal of Mass Spectrometry*, 1999, **193**, 87-99.
42. R. D. Russell, *Journal of Geophysical Research (1896-1977)*, 1971, **76**, 4949-4955.
43. J. F. Rudge, B. C. Reynolds and B. Bourdon, *Chemical Geology*, 2009, **265**, 420-431.
44. N. Belzile and Y.-W. Chen, *Applied Geochemistry*, 2015, **63**, 83-92.
45. M. M. Rahman, C. MacDonald and R. J. Cornett, *Separation Science and Technology*, 2018, **53**, 2055-2063.
46. T. Schirmer, A. Koschinsky and M. Bau, *Chemical Geology*, 2014, **376**, 44-51.
47. J. a. T. D. L. Dedina, *Hydride Generation Atomic Absorption Spectrometry*, Wiley, Chichester, NY, 1995.
48. J. Korkisch, *CRC Handbook of Ion Exchange Resins*, Routledge, 2017.

49. R. Clayton, P. Andersson, N. H. Gale, C. Gillis and M. J. Whitehouse, *Journal of Analytical Atomic Spectrometry*, 2002, **17**, 1248-1256.
50. M. D. Axelsson, I. Rodushkin, J. Ingri and B. Öhlander, *Analyst*, 2002, **127**, 76-82.
51. K. Mitchell, S. Z. Mansoor, P. R. D. Mason, T. M. Johnson and P. Van Cappellen, *Earth and Planetary Science Letters*, 2016, **441**, 178-187.
52. T. Kashiwabara, S. Kubo, M. Tanaka, R. Senda, T. Iizuka, M. Tanimizu and Y. Takahashi, *Geochimica et Cosmochimica Acta*, 2017, **204**, 52-67.
53. M. A. Fehr, M. Rehkämper, A. N. Halliday, U. Wiechert, B. Hattendorf, D. Günther, S. Ono, J. L. Eigenbrode and D. Rumble, *Geochimica et Cosmochimica Acta*, 2005, **69**, 5099-5112.
54. F. Moynier, T. Fujii, P. Telouk and F. Albarede, *Journal of Nuclear Science and Technology*, 2008, **45**, 10-14.

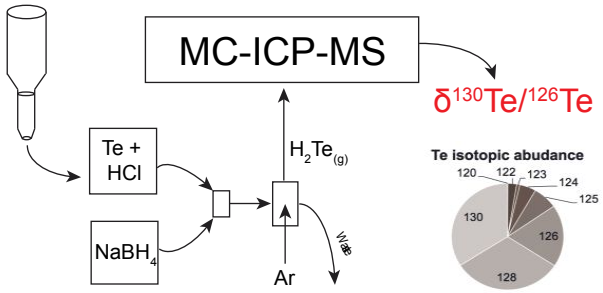

A new method for precise measurements of tellurium stable isotope variations by hydride generation MC-ICP-MS is presented, including a revised sample preparation scheme.